A Time-Domain Approach to Simulation and Characterization of RF HBT Two-Tone Intermodulation Distortion

Kuen Yu Huang, *Student Member, IEEE*, Yiming Li, *Member, IEEE*, and Chien-Ping Lee, *Fellow, IEEE*

***Abstract*—In this paper, we evaluate the two-tone intermodulation distortion for heterojunction bipolar transistors (HBTs) operated at RF. We directly solve the nonlinear differential equations of the HBT large-signal model in time domain by employing the waveform-relaxation and monotone-iterative methods. Based on time-domain results, sinusoidal waveform outputs are transformed into the frequency domain with the fast Fourier transform. Furthermore, the output third-order intercept-point values of the HBT are computed with the spectra. Results for a fabricated InGaP HBT under different testing conditions are reported and compared among the HSPICE results, the results with harmonic balance methodology, and the measured data. Comparisons among these results show that our method demonstrates its superiority over the conventional approaches. This characterization alternative has allowed us to study RF device properties, perform thermal consumption and sensitivity analysis, and extract model parameters.**

***Index Terms*—Distortion, heterojunction bipolar transistor (HBT), intermodulation, output third-order intercept point (OIP3), RF characterization, transient time analysis.**

I. Introduction

HIGH-POWER heterojunction bipolar transistors (HBTs) operated at high frequencies for power amplification have been of great interest for wireless applications in recent years [1]–[5]. One of the favorite properties of HBTs is high linearity. The linearity varies with the device structures and should be optimized with respect to the design of the device structure. For the HBT device linearity, the calculation of two-tone intermodulation distortion is important to characterize the device operated at the RF regime. As is known, different approaches have been proposed to calculate intermodulation distortion [6]–[16]. The most conventional approach for the model problem is with the harmonic balance method, which has been applied for studying large-signal distortion [6]–[8]. The Volterra-series method [9]–[16] has been applied for small-signal distortion when the device is in weak nonlinearity conditions. These two methods are in a class of frequency-domain approaches and have their merits. A method to evaluate two-tone intermodulation is to solve the model problem in the time domain directly. It first performs the analysis with two-tone input excitation. The fast Fourier transform (FFT) is applied to convert the time-domain data into the frequency domain for more analyses and characterizations. However, this exact and straightforward approach (without any approximations) heavily relies on a robust, accurate, and efficient solver. Conventional solution methods applied for solving a set of the nonlinear ordinary differential equations arising from circuit models is the Newton's iterative (NI) method or NI-liked methods. Unfortunately, the NI method is a local method and it converges quadratically in a sufficiently small neighborhood of the exact solution. These properties have their limitation and should be carefully verified in the practical engineering application. It also does not satisfy the requirements of accuracy and stability for intermodulation-distortion analysis.

In this paper, we propose a novel time-domain approach to the calculation and characterization of the two-tone intermodulation distortion. The waveform-relaxation (WR) [17] and monotone-iterative (MI) [18] methods are utilized for solving the large-signal circuit model in time domain. The major property of our solution methodology is solving the nonlinear systems with the MI method instead of the NI method. First of all, a set of nonlinear differential equations are formulated with the Gummel–Poon (GP) model. All equations are decoupled with the WR procedure and solved independently with the MI method. The MI iteration loops will be performed until the computed results meet the convergence criteria. The time-domain results are then analyzed with the FFT to obtain necessary information. The MI method for solving the system of nonlinear algebraic equations arising from semiconductor devices simulation has been proposed and successfully developed earlier by the authors [19]–[21]. The nonlinear model is solved in the time domain without any approximations, thus, the accuracy of the distortion analysis with this method is guaranteed. Based on the method robustness, we significantly reduce the simulation time for the distortion analysis. Various testing conditions for a fabricated InGaP HBT are examined and the characterization results are reported and compared among the HSPICE results, the results of the harmonic balance approach, and the measured data. Our approach demonstrates accurate and robust properties and provides an alternative for RF application.

Manuscript received September 18, 2002; revised January 29, 2003. This work was supported in part by the National Science Council (NSC) of Taiwan, R.O.C., under Contract NSC-90–2215-E-009–056. The work of Y. Li was supported by the NSC under Grant NSC-91–2112-M-317–001 and by the Ministry of Economic Affairs, Taiwan, R.O.C., under Grant PSOC 91-EC-17-A-07-S1–0011.

K. Y. Huang and C.-P. Lee are with the Department of Electronics Engineering, National Chiao Tung University, Hsinchu 300, Taiwan, R.O.C.

Y. Li is with the Department of Nano Device Technology, National Nano Device Laboratories, Hsinchu 300, Taiwan, R.O.C. and also with the Microelectronics and Information Systems Research Center, National Chiao Tung University, Hsinchu 300, Taiwan, R.O.C. (e-mail: ymli@mail.nctu.edu.tw).

Digital Object Identifier 10.1109/TMTT.2003.817681

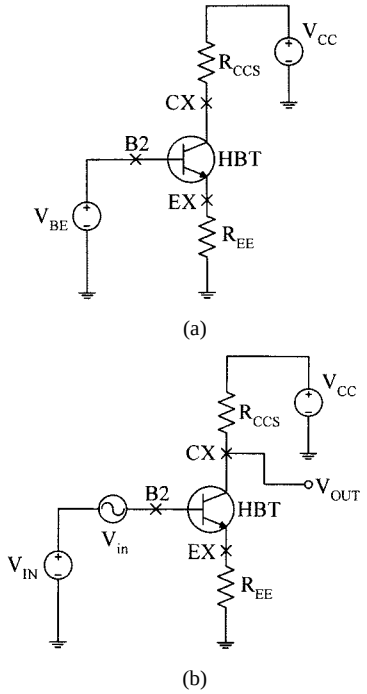

Fig. 1. (a) Circuit for dc simulation. (b) Applied circuit for two-tone intermodulation simulation.

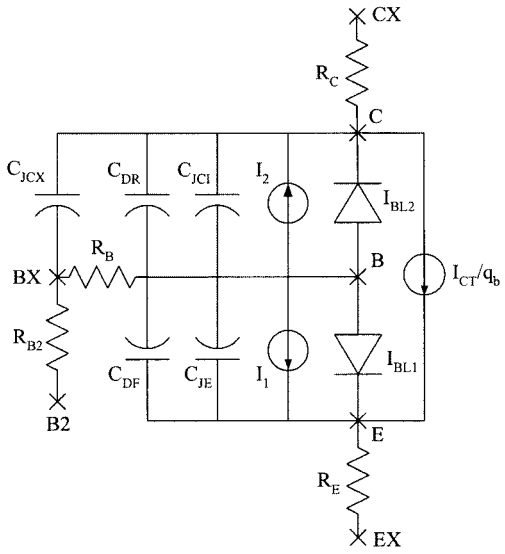

Fig. 2. GP large-signal equivalent-circuit model.

Subsequent sections of this paper are organized as follows. Section II introduces the model and characterization method. Section III describes results of calculations; various comparisons and analyses are also presented in detail. Section IV presents the conclusion.

II. Model for HBT Characterization

Fig. 1 shows the HBT circuit in the dc and RF characterizations, where $V_{\rm IN}$ is the dc-bias voltage and $V_{\rm in}$ is the two-tone input signal. We express $V_{\rm in}$ in the following form:

$$V_{\rm in} = V_m\big(\cos(\omega_1 t) + \cos(\omega_2 t)\big) \tag{1}$$

TABLE I
SET OF InGaP HBT PARAMETERS FOR THE GP MODEL

Notation	Value	Unit
IS	2.85E-24	A
BF	86.95	-
NF	1.068	-
IKF	0.1815	A
IKR	1.032E-3	A
ISE	2.34E-18	A
NE	1.91	-
BR	1.47	-
NR	1.06	-
ISC	2.142E-14	A
NC	1.954	-
RB	48.13	Ohm
RB2	8.75	Ohm
RE	1.256	Ohm
RC	6.75	Ohm
CJEO	130.0E-15	F
VJE	1.367	V
MJE	0.1188	-
TF	2.680E-12	Sec
XTF	275.6	-
VTF	66.0	-
CJCO	24.27E-15	F
VJC	0.7161	V
MJC	0.266	-
XCJC	0.3428	-
TR	350.0E-12	Sec
ITF	419.80E-3	A
FC	0.5	-

where $\omega_1 = 2\pi f_1$ and $\omega_2 = 2\pi f_2$ are two different frequencies and V_m is the amplitude of tones.

As shown in Fig. 2, we formulate a set of time-dependent nodal equations with the GP large-signal model [22], [23]. At the nodes of EX and CX, time-independent algebraic equations are formulated. The nodal equations of equivalent circuit by Kirchhoff's current law (KCL) are as follows:

$$\begin{aligned} &C_{JCX}\left(\frac{dV_{BX}}{dt} - \frac{dV_C}{dt}\right) + C_{DR}\left(\frac{dV_B}{dt} - \frac{dV_C}{dt}\right) \\ &\quad + C_{JCI}\left(\frac{dV_B}{dt} - \frac{dV_C}{dt}\right) + I_2 + I_{BL2} \\ &\quad - \frac{I_{CT}}{q_b} + \frac{V_{CX} - V_C}{R_C} \\ &\quad = 0 \end{aligned} \tag{2}$$

$$\begin{aligned} &C_{DF}\left(\frac{dV_B}{dt} - \frac{dV_E}{dt}\right) + C_{JE}\left(\frac{dV_B}{dt} - \frac{dV_E}{dt}\right) \\ &\quad + I_1 + I_{BL1} + \frac{I_{CT}}{q_b} + \frac{V_{EX} - V_E}{R_E} \\ &\quad = 0 \end{aligned} \tag{3}$$

$$\begin{aligned} &C_{DR}\left(\frac{dV_B}{dt} - \frac{dV_C}{dt}\right) + C_{JCI}\left(\frac{dV_B}{dt} - \frac{dV_C}{dt}\right) \\ &\quad + C_{DF}\left(\frac{dV_B}{dt} - \frac{dV_E}{dt}\right) + C_{JE}\left(\frac{dV_B}{dt} - \frac{dV_E}{dt}\right) \\ &\quad + I_1 + I_{BL1} + I_2 + I_{BL2} + \frac{V_B - V_{BX}}{R_B} \\ &\quad = 0 \end{aligned} \tag{4}$$

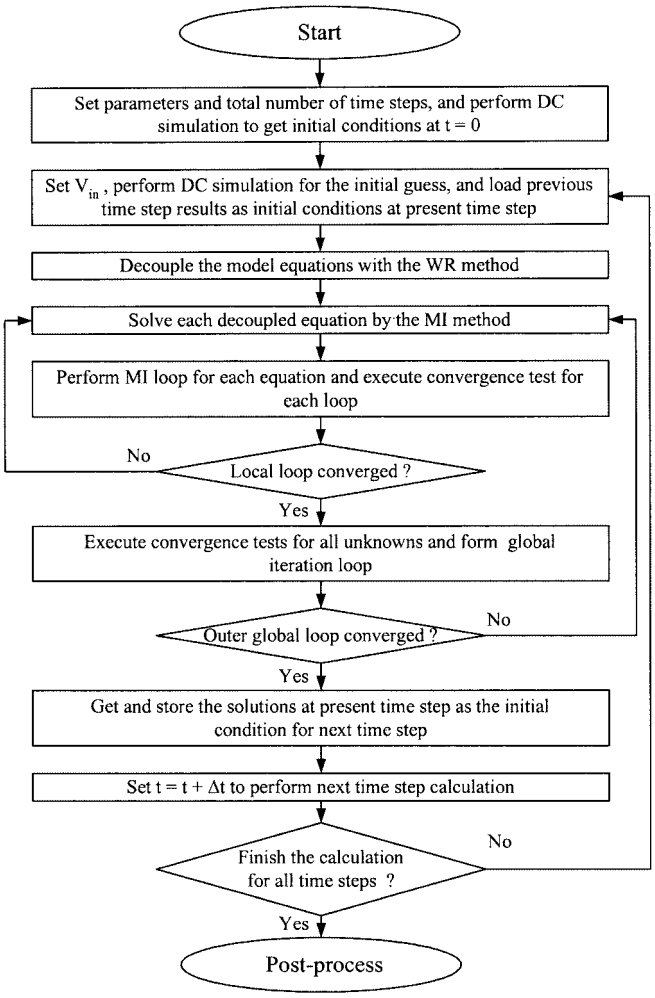

Fig. 3. Flowchart of the proposed solution method.

$$C_{JCX}\left(\frac{dV_C}{dt}-\frac{dV_{BX}}{dt}\right)+\frac{V_B-V_{BX}}{R_B}+\frac{(V_{\rm IN}+V_{\rm in})-V_{BX}}{R_{B2}}=0 \tag{5}$$

$$\frac{V_C-V_{CX}}{R_C}+\frac{V_{CC}-V_{CX}}{R_{CCS}}=0 \tag{6}$$

$$\frac{V_E-V_{EX}}{R_E}-\frac{V_{EX}}{R_{EE}}=0. \tag{7}$$

All the current and capacitor terms in the GP model are functions of bias conditions, with the GP model parameters of the InGaP HBT used in this paper shown in Table I.

Fig. 3 presents a flowchart for the proposed WR and MI solution technique in the time domain. Referring to the flowchart, we first set the necessary parameters for the circuit model. The total number of time steps to be solved and the time-step size Δt are also determined. We compute the dc (steady state) results, which are used for the initial conditions of the time evolution when the RF signal $V_{\rm in}$ is inputted. At each time step, the calculated results of the previous time step are used for the initial conditions at the present time-step simulation. Our computational procedure includes six MI solution loops and a global-iteration loops to reach the convergent results. The convergence tests are for each MI loop, as well as the global outer loops. After the convergence tests for all MI loops, we check the convergence for all unknown variables in the outer loop (the so-called global-iteration loop). Once the convergence requirements for all unknowns are satisfied at the same global-iteration loop, we output the computed solutions at the present time step. These solutions are then used for the initial conditions at the next time step. If all of the time steps have been solved, we use the time-domain results with the two-tone excitation input to perform the distortion analysis.

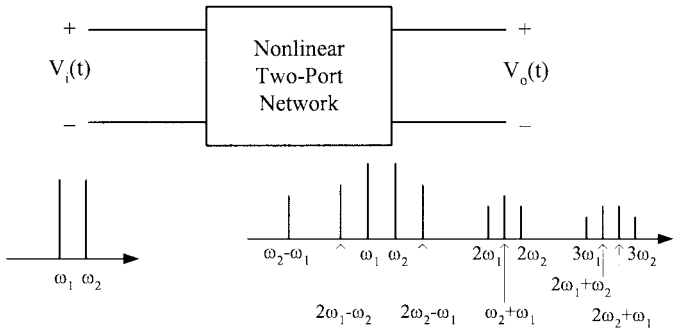

Fig. 4. Illustration of two-tone intermodulation characteristics for a nonlinear two-port network.

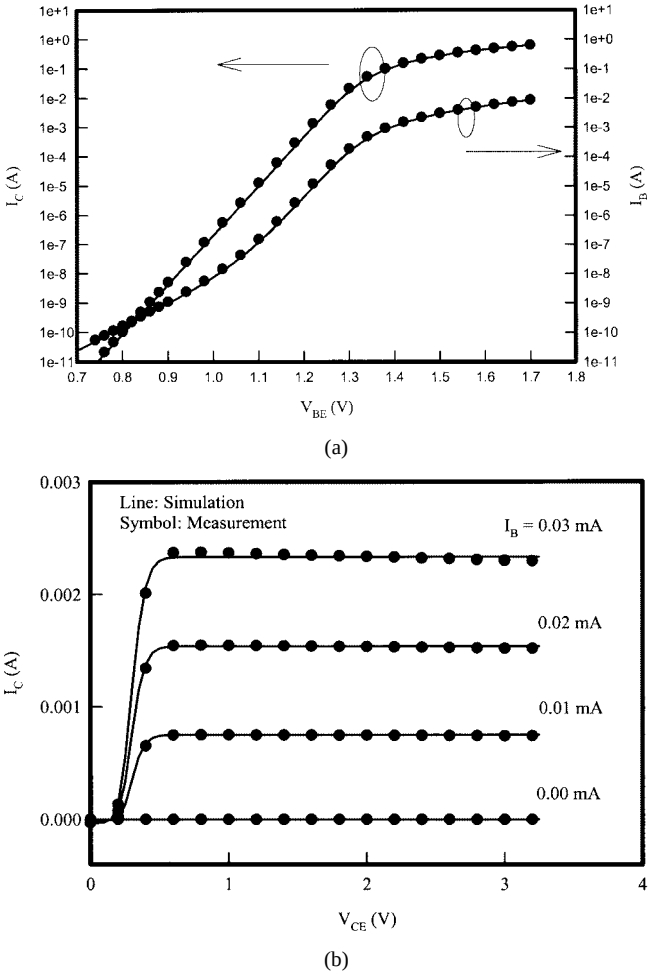

Fig. 5. (a) Gummel plot. (b) I_C–$V_{\rm BE}$ dc curves of the InGaP HBT circuit.

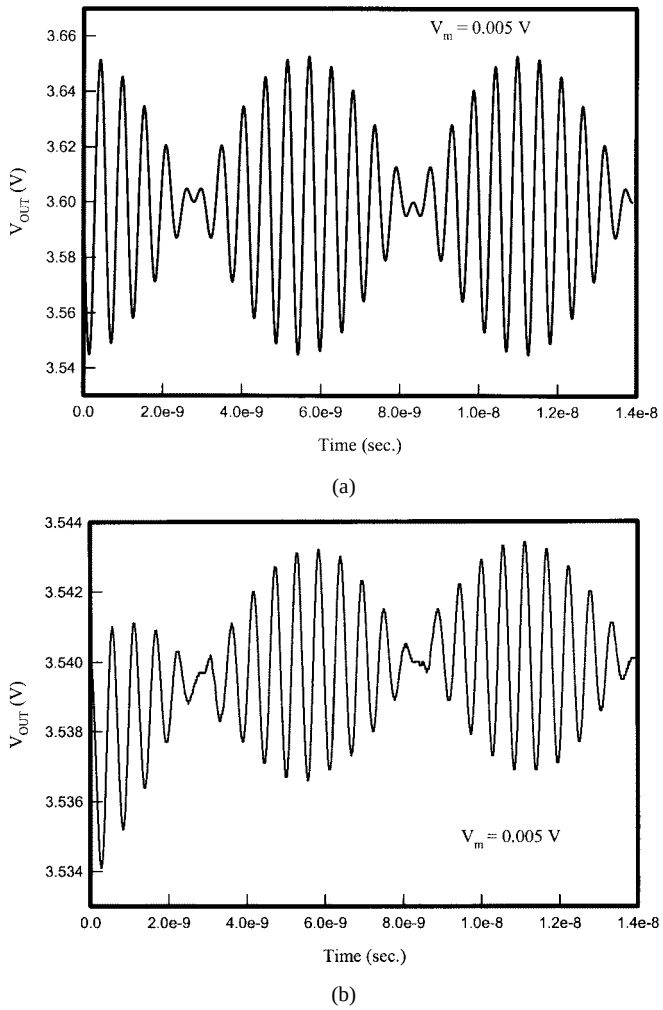

Fig. 6. Comparison of $V_{\rm OUT}$ between: (a) our solver and (b) the HSPICE simulator, where the input power is set to be -3 dBm.

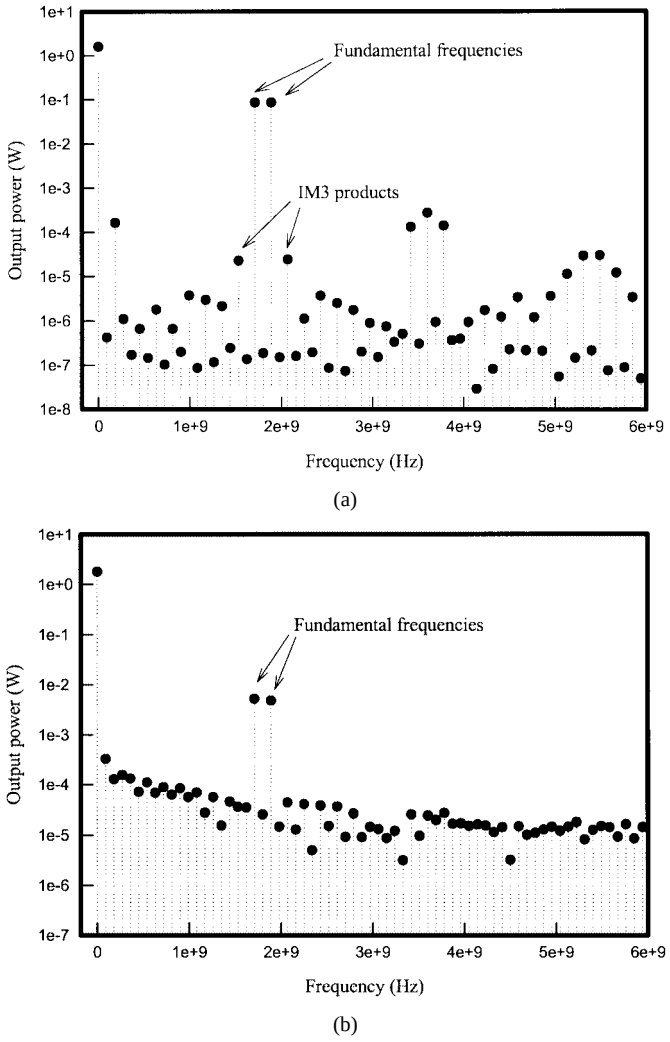

Fig. 7. Plots of the output power spectrum for: (a) our results and (b) HSPICE results.

We extract the intensity of amplitude or power at a specified frequency from the FFT results using the computed data in the time domain. When a two-tone input signal $V_{\rm in}$ is applied to a nonlinear two-port network whose output signal can be represented by the power series

$$V_o = a_1 V_{\rm in}(t) + a_2\big(V_{\rm in}(t)\big)^2 + a_3\big(V_{\rm in}(t)\big)^3. \qquad (8)$$

Fig. 4 shows the spectrums of input and output signals. The harmonics are found close to the fundamental frequencies. The third-order intermodulation (IM3) products play an important role for the intermodulation linearity of HBT devices. We note the output amplitudes of fundamental frequencies and IM3 products are $a_1 V_m$ and $3a_3 V_m^3/4$, and the slopes of the plotted lines versus V_m equal 1 and 3 in log scale. The value of the output third-order intercept point (OIP3) is the projection of the cross point of these two extrapolated lines. It is an important benchmark to evaluate the linearity of the devices at frequency modulation. The value of OIP3 depends on the device material and the design of the device structures. In general, the higher OIP3 value represents the better linearity of the two-tone intermodulation characteristics.

III. Results and Discussion

An InGaP HBT device is fabricated and measured in this work. Fig. 5(a) shows the Gummel plot of the InGaP HBT, where the lines denote our results with the new method and the symbols denote HSPICE results. Both of them have consistency in the dc condition. Fig. 5(b) is the calculated I_C–$V_{\rm BE}$ curves together with the measured data of the InGaP HBT, and the result is quite in agreement with measurement. Fig. 5 primarily confirms the proposed method has its accuracy in dc analysis. As shown in Fig. 1(b), Fig. 6 demonstrates the time-domain result of the output voltage ($V_{\rm OUT}$). Over 25 periods are directly calculated in the time domain with the input two-tone excitations. The input signal amplitude denoted as V_m equals 0.005 V. The fundamental frequencies f_1 and f_2 are 1.71 and 1.89 GHz, respectively. Fig. 6(a) and (b) presents our results and the HSPICE results, respectively. Contrary to the HSPICE results, which initially have some unstable outputs, our simulator presents its robustness in the large-signal time-domain analysis.

With the time-domain results shown in Fig. 6(a) and (b), we calculate the spectrums of the output power by the FFT directly. Fig. 7(a) and (b) is the corresponding spectra with Fig. 6(a) and (b), respectively. In computing Fig. 7(a),

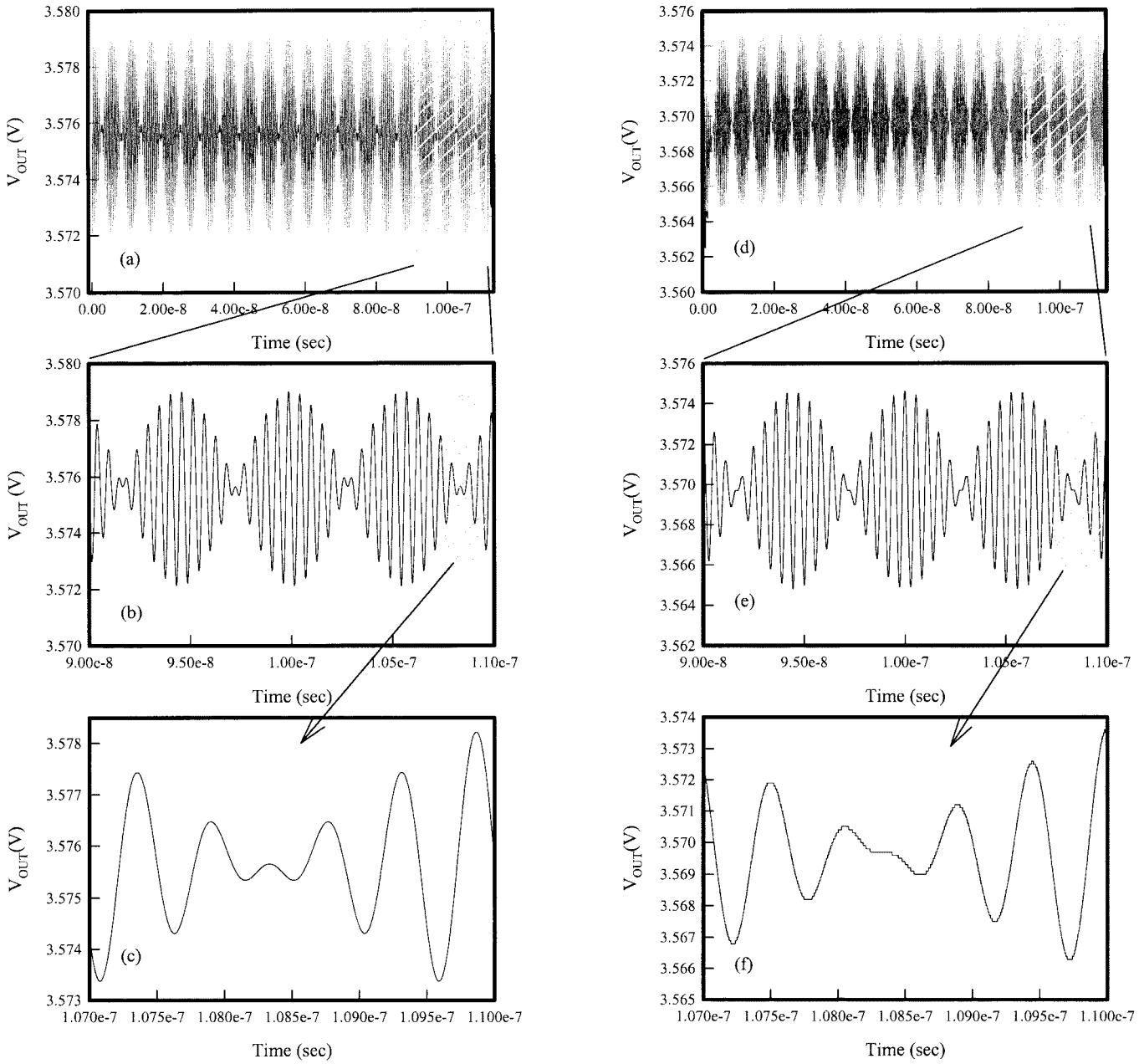

Fig. 8. Zoom-in plots investigation and comparison of $V_{\rm out}$ between: (a)–(c) our solver and (d)–(f) the HSPICE simulator.

our simulated data is beginning from the time 0.556 ns (1 cycle$^*(1/f_c) = 1/1.8$ GHz $= 0.556$ ns). In Fig. 7(b), we performed the FFT with the HSPICE results beginning from the time 8.33 ns (15 cycles$^*(1/f_c) = 15/1.8$ GHz $= 8.33$ ns) and forward. We find the IM3 products at $2f_1 - f_2$ and $2f_2 - f_1$ are clearly observed in Fig. 7(a). However, as shown in Fig. 7(b), it is difficult to identify the two IM3 products. Our methodology for large-scale time-domain analysis and two-tone intermodulation demonstrates its superiority over some approaches. As shown in Fig. 8(a)–(f), to clarify the time-domain results calculated with HSPICE and our approach, we have performed more computational investigations. It is found that, as shown in Fig. 8(d)–(f), the outputs of the HSPICE simulator are erroneous results (marked) until 100 ns outputted. The input signal applied in this testing is with $V_m = 0.05$ V, $V_{\rm BE} = 1.402$ V, and $V_{\rm CE} = 3.6$ V.

The IM3 products at $2f_2 - f_1$ and $2f_1 - f_2$ are denoted as HI-IM3 and LO-IM3, respectively. Fig. 9 is the output powers at the fundamental frequencies and the IM3 products versus the input power. As shown in Fig. 9(a), our calculated slopes are 0.99726 and 3.00606 in that they are almost equal to the theoretical values of 1 and 3, respectively. We note that the HI-IM3 and LO-IM3 are closed enough and, hence, HI-IM3 and LO-IM3 almost have the same OIP3 value at 36.9 dBm. Unfortunately, as shown in Fig. 9(b), the slopes of the fundamental frequencies and IM3 products from the HSPICE results equal 0.99964 and -0.28781, respectively. It leads to a nonpredictable OIP3 value with the HSPICE results from time-domain analysis.

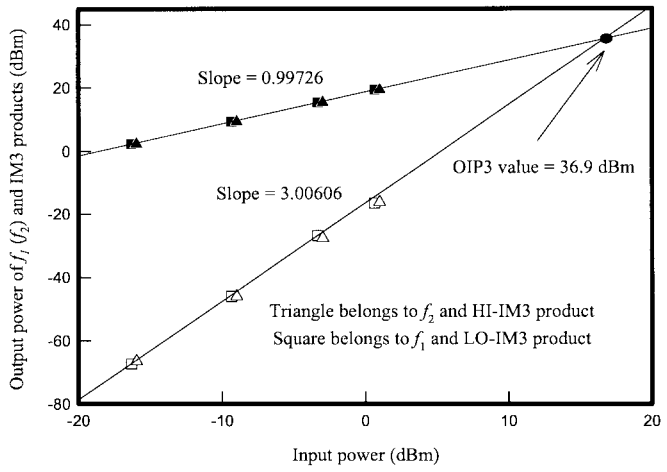

(a)

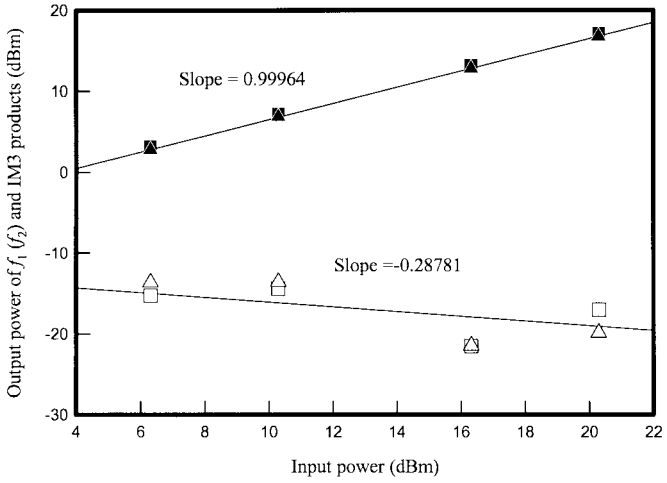

(b)

Fig. 9. Output power at f_0 (black-filled symbol) and the IM3 products (white-filled symbol) versus the input power. (a) Our result. (b) HSPICE result.

For an input power, we can also calculate the OIP3 value with the output power spectrum. If the slopes of the fundamental frequencies and IM3 products are 1.0 and 3.0, the OIP3 value is directly given by

$$\text{OIP3} = P_o^{\text{ff.}} + \frac{1}{2}\left(P_o^{\text{ff.}} - P_o^{\text{IM}_3}\right) \tag{9}$$

where $P_o^{\text{ff.}}$ and $P_o^{\text{IM}_3}$ are the output powers of the fundamental frequencies and IM3 products, respectively. Fig. 10 shows the OIP3 with respect to different spacing ($\Delta f = f_1 - f_2$) of fundamental frequency, where the central frequency $f_c = 1/2(f_1 + f_2)$ of each OIP3 calculation is identical and equals 1.8 GHz. As shown in Fig. 10, there are only slight deviations of OIP3 versus Δf. Variation of Δf from 360 to 20 MHz produces 0.0180-dBm difference in the LO-OIP3 value (36.5294–36.5014). In addition, the differences between LO-OIP3 and HI-OIP3 are 0.0719 and 0.0034782 dBm when the variations are from 360 to 20 MHz. With this observation, our approach enables us to efficiently calculate the intermodulation distortion with a larger Δf. For example, for $\Delta f = 20$ MHz, we have to perform the computation with over 180 periods for FFT transformation. On the other hand, for $\Delta f = 360$ MHz, there are only ten periods required. From

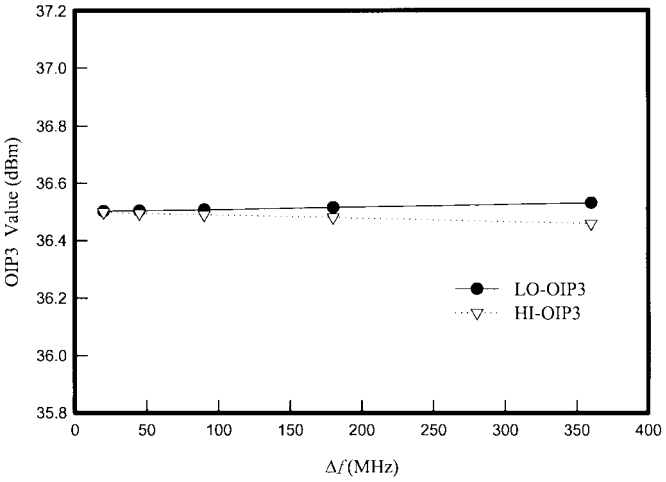

Fig. 10. Deviation plot of OIP3 versus Δf.

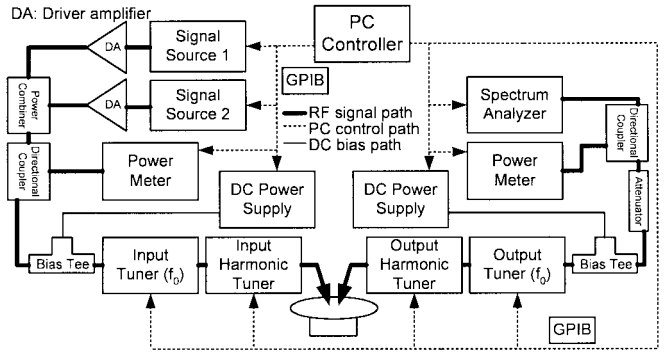

Fig. 11. Setup of on-wafer device testing with harmonic load–pull system.

our numerical experience, we would like to point out that our approach can compute it with a narrow tone spacing of 10 MHz. In our practical implementation, this method provides a more efficient computing alternative and may significantly overcome one of the weaknesses of the conventional time-domain approaches, such as the enormous computational resources. For a typical distortion characterization test, we have successfully reduced the simulation CPU time up to one order of magnitude.

In the investigation of Fig. 10 above, the setup of on-wafer device testing with a harmonic load–pull system has been constructed [24], as shown in Fig. 11. The setting of load–pull systems and a proper pre-calibration procedure enable us to measure the input and output power and the intermodulation property from the device itself directly. For the numerical calculation presented in this paper (the circuits shown in Figs. 1 and 2), we focus on the properties coming from the equivalent circuit of the device. The impedance match problem is ignored and the system is assumed to be an ideal circuit.

Fig. 12(a) shows the OIP3 values versus collector current density J_c. Our results of HI-OIP3 (dotted line) and LO-OIP3 (solid line) are a coincidence. Compared with the measured data (squares), our results indicate their accuracy for different biases. Fig. 12(b) plots the *HP ADS* (a well-known harmonic balance based circuit solver[1] [25]–[27]) results and measure-

[1]*Advanced Design System (ADS) Simulator*, Hewlett-Packard Company, Palo Alto, CA. [Online]. Available: http://eesof.tm.agilent.com/products/

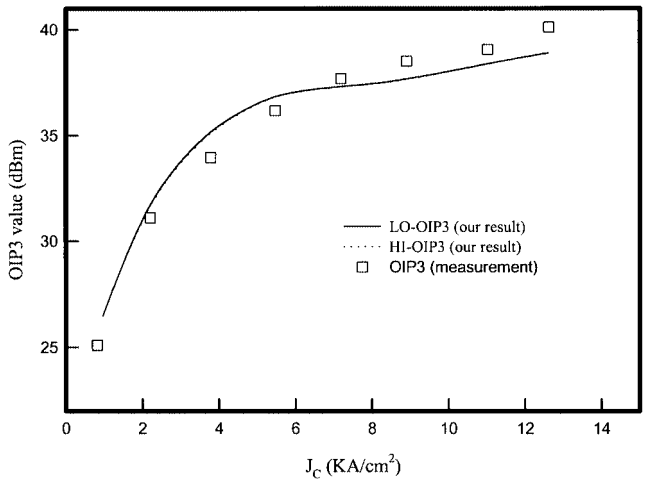

(a)

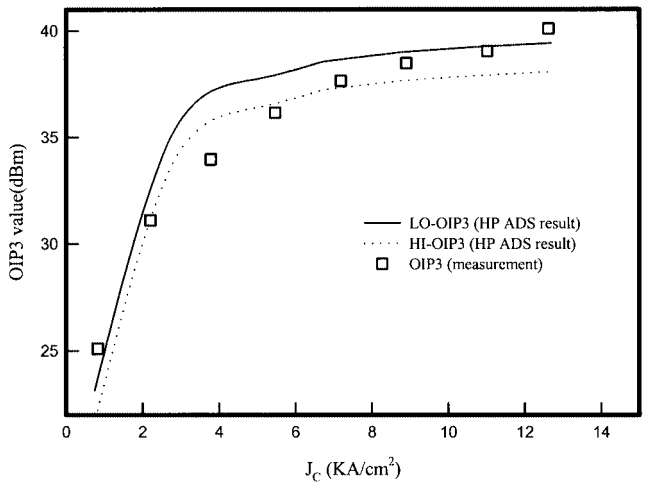

(b)

Fig. 12. OIP3 versus J_c. (a) Measurement and our simulations. (b) Measurement and results with the harmonic balance method.

ment. We find there is over a 1-dBm difference between the values of HI-OIP3 and LO-OIP. Our measurement is performed on a $2.8 \times 12\ \mu\text{m}^2 \times 104$ fingers power amplifier. A multiplier $\text{M} = 104$ is adopted in both the HSPICE and our simulations. In our simulations with *HP ADS*, we find that both of the differences for HI-OIP3 and LO-OIP3 always exist and cannot be further improved to match the measured data well at the same time.

IV. Conclusions

We have evaluated and characterized two-tone intermodulation distortion for the InGaP HBT device operated in RFs. For theoretical investigations of an RF HBT circuit distortion, the developed method has demonstrated its superiority over the conventional one. Simulation results of the InGaP HBT have been reported to show the accuracy and stability of this method. Compared with the results from the HSPICE simulator and the HP ADS simulator (harmonic balance approach), our results not only had good agreement with the measured data, but also presented excellent computational efficiency in characterization of RF HBT two-tone intermodulation distortion.

References

[1] P. M. Asbeck *et al.*, "Heterojunction bipolar transistors for microwave and millimeter-wave integrated circuits," *IEEE Trans. Electron Devices*, vol. ED-34, pp. 2571–2579, Dec. 1987.

[2] M. Yanagihara *et al.*, "High $f_{\max}$ AlGaAs/GaAs HBT with L-shaped base electrode and its application to 50 GHz amplifier," *Solid State Electron.*, vol. 41, pp. 1615–1620, 1997.

[3] N. Pan *et al.*, "High reliability InGaP/GaAs HBT," *IEEE Trans. Electron Devices*, vol. 19, pp. 115–117, Apr. 1998.

[4] Y. S. Lee and C. S. Park, "Structural optimization of InGaP/GaAs HBT for power amplifier applications," in *Proc. IEEE RAWCON*, 2001, pp. 249–252.

[5] T. Oka *et al.*, "High-speed small-scale InGaP/GaAs HBT technology and its application to integrated circuits," *IEEE Trans. Electron Devices*, vol. 48, pp. 2625–2630, Nov. 2001.

[6] K. S. Kundert *et al.*, *Steady-State Method for Simulating Analog and Microwave Circuit*. Norwell, MA: Kluwer, 1990.

[7] B. Li and S. Prasad, "Harmonic and two-tone intermodulation distortion analyses of the inverted InGa/InAlAs/InP HBT," *IEEE Trans. Microwave Theory Tech.*, vol. 45, pp. 1135–1137, July 1997.

[8] B. Troyanovsky *et al.*, "Physics-based simulation of nonlinear distortion in semiconductor devices using the harmonic balance method," *Comput. Methods Appl. Mech. Eng.*, vol. 181, pp. 467–482, 2000.

[9] P. Wambacq and W. Sansen, *Distortion Analysis of Analog Integrated Circuit*. Norwell, MA: Kluwer, 1998.

[10] S. A. Maas *et al.*, "Intermodulation in heterojunction bipolar transistors," *IEEE Trans. Microwave Theory Tech.*, vol. 40, pp. 442–448, Mar. 1992.

[11] A. Samelis and D. Pavlidis, "Mechanisms determining third order intermodulation distortion in AlGaAs/GaAs heterojunction bipolar transistors," *IEEE Trans. Microwave Theory Tech.*, vol. 40, pp. 2374–2380, Dec. 1992.

[12] J. Lee *et al.*, "Intermodulation mechanism and linearization of AlGaAs/GaAs HBT's," *IEEE Trans. Microwave Theory Tech.*, vol. 45, pp. 2065–2072, Dec. 1997.

[13] B. Li and S. Prasad, "Intermodulation analysis of the collector-up InGaAs/InAlAs/InP HBT using Volterra series," *IEEE Trans. Microwave Theory Tech.*, vol. 46, pp. 1321–1323, Sept. 1998.

[14] M. Iwamoto *et al.*, "Linearity characteristics of GaAs HBT's and the influence of collector design," *IEEE Trans. Microwave Theory Tech.*, vol. 48, pp. 2377–2388, Dec. 2000.

[15] G. Niu *et al.*, "Systematic analysis of RF distortion in SiGe HBT's," in *IEEE RFIC Symp. Dig.*, 2001, pp. 147–150.

[16] Y. Wang *et al.*, "Asymemetry in intermodulation distortion of HBT power amplifiers," in *IEEE GaAs IC Symp. Tech. Dig.*, 2001, pp. 201–204.

[17] E. Lelarasmee *et al.*, "The waveform relaxation method for time-domain analysis of large scale integrated circuits," *IEEE Trans. Computer-Aided Design*, vol. CAD-1, pp. 131–145, July 1982.

[18] Y. Li, "A monotone iterative method for bipolar junction transistor circuit simulation," *WSEAS Trans. Math.*, vol. 1, pp. 159–164, Oct. 2002.

[19] ——, "A new parallel adaptive finite volume method for the numerical simulation of semiconductor devices," *Comput. Phys. Commun.*, vol. 142, pp. 285–289, Dec. 2001.

[20] ——, "A practical implementation of parallel dynamic load balancing for adaptive computing in VLSI device simulation," *Eng. Comput.*, vol. 18, pp. 124–137, Aug. 2002.

[21] ——, "A monotone iterative method for semiconductor device drift diffusion equations," *WSEAS Trans. Syst.*, vol. 1, pp. 68–73, Jan. 2002.

[22] L. E. Getreu, *Modeling the Bipolar Transistor*. Amsterdam, The Netherlands: Elsevier, 1984.

[23] W. Liu, *Handbook of III–V Heterojunction Bipolar Transistor*. New York: Wiley, 1998.

[24] E. Alekseev, D. Pavlidis, and C. Tsironis, "W-band on-wafer load–pull measurement system and its application to HEMT characterization," in *IEEE MTT-S Int. Microwave Symp. Dig.*, 1998, pp. 1479–1482.

[25] W. Ryu *et al.*, "Over GHz low-power RF clock distribution for a multiprocessor digital system," in *Proc. IEEE Electronic Components Technology Conf.*, 2001, pp. 133–140.

[26] L. Dermentzoglou *et al.*, "A direct conversion receiver analysis for multistandard wireless applications," in *Proc. 10th IEEE Mediterranean Electrotechnical Conf.*, 2000, pp. 318–321.

[27] R. Follmann *et al.*, "A universal method for calculating and extracting the LF and RF noise behavior of nonlinear devices," in *Proc. 22nd IEEE Annu. GaAs IC Symp.*, 2000, pp. 47–51.

Kuen Yu Huang (S'99) was born in Kaohsiung, Taiwan, R.O.C., in 1973. He received the B.S. degree in electrical engineering from the National Tsing-Hua University, Hsinchu, Taiwan, R.O.C., in 1996, the M.S. degree in electronics engineering from the National Chiao Tung University (NCTU), Hsinchu, Taiwan, R.O.C., in 1998, and is currently working toward the Ph.D. degree in electronics engineering at NCTU.

His research interests include modeling and simulation of high-frequency devices and nonlinear circuits.

Mr. Huang is a student member of the IEEE Microwave Theory and Technique Society (IEEE MTT-S), the IEEE Electron Devices Society, and the IEEE Solid-State Circuits Society.

Yiming Li (M'02) received the B.S. degrees in applied mathematics and electronics engineering, M.S. degree in applied mathematics, and Ph.D. degree in electronics from the National Chiao Tung University, Taiwan, R.O.C., in 1996, 1998, and 2001, respectively.

In 2001, he joined the National Nano Device Laboratories (NDL), Taiwan, R.O.C., as an Associate Researcher, and the Microelectronics and Information Systems Research Center, National Chiao Tung University, as an Assistant Professor, where he has been engaged in the research and development of modeling and simulation of nanodevices and very large scale integration (VLSI) circuits. In Fall 2002, he was a Visiting Assistant Professor with the Department of Electrical and Computer Engineering, University of Massachusetts at Amherst. He is the Research Consultant of the System on a Chip (SoC) Technology Center, Industrial Technology Research Institute (ITRI), Hsinchu, Taiwan, R.O.C. He is the Director of the Department of Nano Device Technology, NDL, and conducts the Nanodevice Technology Computer-Aided Design (TCAD) Laboratory and the Parallel and Scientific Computing Laboratory at the NDL and NCTU. His current research areas include computational electronics and physics, physics of semiconductor nanostructures, device modeling and parameter extraction, VLSI and RF circuit simulation, bioinformatics and computational biology, advanced numerical method, parallel and scientific computation and computational intelligence, and the development of TCAD/Electronic Computer-Aided Design (ECAD) tools and SoC applications. He has authored or coauthored over 90 research papers appearing in international books, journals, and conferences.

Dr. Li is a member of Phi Tau Phi, the American Physical Society, the Institute of Electronics, Information and Communication Engineers, the Society for Industrial and Applied Mathematics, and the World Scientific and Engineering Academy and Society. He was the recipient of the 2002 Research Fellowship Award presented by the Pan Wen-Yuan Foundation, Taiwan, R.O.C.

Chien-Ping Lee (M'80–SM'94–F'00) received the B.S. degree in physics from the National Taiwan University, Taipei, Taiwan, R.O.C., in 1971, and the Ph.D. degree in applied physics from the California Institute of Technology, Pasadena, in 1978.

He was with Bell Laboratories and later with Rockwell International until 1987. While at Rockwell International, he was a Department Manager, where he was responsible for the development of high-speed semiconductor devices. In 1987, he became a Professor with the National Chiao Tung University, Hsinchu, Taiwan, R.O.C. He was also appointed Director of the Semiconductor Research Center and, later, the first Director of the National Nano Device Laboratory. He is currently the Director of the Nano Science and Technology Center, National Chiao Tung University. He is well recognized in the field of semiconductor research. He is an expert in compound semiconductor devices and was the pioneer of the development of opto-electronic integrated circuits (OEICs), high electron-mobility transistors (HEMTs), and ion-implanted MESFETs. His current interests include semiconductor nanostructures, quantum devices, spintronics, and HBTs. He has graduated 20 Ph.D. students and over 40 Master's degree students.

Dr. Lee was the founding chair of the IEEE Lasers and Electro-Optics Society (LEOS) Taipei Chapter and has also served in the IEEE Electron Devices Society (EDS) Taipei Chapter. He has organized and served on several international conferences. He was the recipient of the 1982 Engineer of the Year Award presented by Rockwell International, the 1993 Best Teacher Award presented by the Ministry of Education, the 2000 Outstanding Engineering Professor Award presented by the Chinese Institute of Engineers, the 1993, 1995, and 1997 Outstanding Research Award presented by the National Science Council, the 2000 Outstanding Scholar Award presented by the Foundation for the Advancement of Outstanding Scholarship, and the 2001 Academic Achievement Award presented by the Ministry of Education.